Earth Surf. Dynam., 7, 191–197, 2019
https://doi.org/10.5194/esurf-7-191-2019

Earth Surface Dynamics
Open Access
EGU

Aging of basalt volcanic systems and decreasing CO_2 consumption by weathering

Janine Börker[1], Jens Hartmann[1], Gibran Romero-Mujalli[1], and Gaojun Li[2]

[1]Institute for Geology, CEN (Center for Earth System Research and Sustainability), Universität Hamburg, Bundesstraße 55, 20146 Hamburg, Germany
[2]MOE Key Laboratory of Surficial Geochemistry, Department of Earth Sciences, Nanjing University, 163 Xianlindadao, Nanjing 210023, China

Correspondence: Janine Börker (janine.boerker@uni-hamburg.de), Jens Hartmann (geo@hattes.de)

Received: 1 February 2018 – Discussion started: 22 March 2018
Revised: 9 November 2018 – Accepted: 4 December 2018 – Published: 6 February 2019

Abstract. Basalt weathering is one of many relevant processes balancing the global carbon cycle via land–ocean alkalinity fluxes. The CO_2 consumption by weathering can be calculated using alkalinity and is often scaled with runoff and/or temperature. Here, it is tested if the surface age distribution of a volcanic system derived by geological maps is a useful proxy for changes in alkalinity production with time.

A linear relationship between temperature normalized alkalinity fluxes and the Holocene area fraction of a volcanic field was identified using information from 33 basalt volcanic fields, with an $r^2 = 0.93$. This relationship is interpreted as an aging function and suggests that fluxes from Holocene areas are ~ 10 times higher than those from old inactive volcanic fields. However, the cause for the decrease with time is probably a combination of effects, including a decrease in alkalinity production from material in the shallow critical zone as well as a decline in hydrothermal activity and magmatic CO_2 contribution. The addition of fresh reactive material on top of the critical zone has an effect in young active volcanic settings which should be accounted for, too.

A comparison with global models suggests that global alkalinity fluxes considering Holocene basalt areas are $\sim 60\,\%$ higher than the average from these models imply. The contribution of Holocene areas to the global basalt alkalinity fluxes is today however only $\sim 5\,\%$, because identified, mapped Holocene basalt areas cover only $\sim 1\,\%$ of the existing basalt areas. The large trap basalt proportion on the global basalt areas today reduces the relevance of the aging effect. However, the aging effect might be a relevant process during periods of globally intensive volcanic activity, which remains to be tested.

1 Introduction

Basalt areas, despite their limited areal coverage, contribute significantly to CO_2 sequestration by silicate rock weathering (Gaillardet et al., 1999; Dessert et al., 2003; Hartmann et al., 2009). The sensitivity of basalt weathering to climate change (Dessert et al., 2001, 2003; Coogan and Dosso, 2015; Li et al., 2016) supports a negative weathering feedback in the carbon cycle that maintains the habitability of the Earth's surface over geological timescales (Walker et al., 1981; Berner et al., 1983; Li and Elderfield, 2013). Changes in volcanic weathering fluxes due to emplacement of large volcanic provinces or shifts in the geographic distribution of volcanic fields associated with continental drift may have contributed to climate change in the past (Goddéris et al., 2003; Schaller et al., 2012; Kent and Muttoni, 2013).

The role of basalt weathering in the carbon cycle and its feedback strength in the climate system depends, besides the release of geogenic nutrients, on the amount of associated CO_2 consumption and related alkalinity fluxes. The factors that modulate these fluxes are a subject of uncertainty. Previous studies suggest that basalt weathering contributes 25 %–35 % to the global silicate CO_2 consumption by weathering (Gaillardet et al., 1999; Dessert et al., 2003; Hartmann et al., 2009). However, their estimations do not consider the po-

tential aging of a weathering system (e.g., Taylor and Blum, 1995). Young volcanic areas can show much higher weathering rates compared to older ones, as was shown for the Lesser Antilles, where a rapid decay of weathering rates within the first 0.5 Ma was observed (Rad et al., 2013). Such an aging effect of volcanic areas is difficult to parameterize for global basalt weathering fluxes, due to a lack of global compilations.

A practical approach to resolve this issue is to distinguish older and inactive volcanic fields (IVFs) and active volcanic fields (AVFs) (Li et al., 2016) and compare weathering fluxes with factors driving the weathering process, like land surface temperature or hydrological parameters. By compiling data from 37 basaltic fields globally, Li et al. (2016) showed that spatially explicit alkalinity fluxes (or CO_2 consumption rates) associated with basalt weathering correlate strongly with land surface temperature for IVFs but not for AVFs. They suggested that previously observed correlations between weathering rates and runoff in global datasets originate partly from the coincidence of high weathering rates and high runoff of AVFs rather than a direct primary runoff control on the weathering rate. Many studied AVFs are located near the oceans and have an elevated topography, a combination which can cause elevated runoff due to an orographic effect (Gaillardet et al., 2011). However, the effect of aging on weathering rates from a volcanic system discussed here has not been evaluated.

The age distribution of the surface area of a whole volcanic system might be used as a first-order proxy to study the variability of weathering fluxes of AVFs. However, the exact surface age of volcanic areas is rarely mapped in detail, but Holocene areas are often reported in geological maps. Here, basalt alkalinity fluxes are related to the calculated Holocene areal proportion of volcanic fields at the catchment scale. For this, the concept of weathering reactivity is introduced, which is the relative alkalinity flux of AVFs to the alkalinity flux estimated for IVFs. This reactivity (R) is compared with the relative age distribution of surface areas, using the proportion of total area occupied by Holocene lavas. From this comparison, a function for the decay of alkalinity fluxes with increasing proportion of older land surface area is derived and discussed.

2 Methods

The volcanic fields used to establish the relationship between weathering reactivity and Holocene coverage are predominantly described as basalt areas (Li et al., 2016). Based on the availability of detailed geological maps, 33 volcanic provinces were selected, with 19 IVFs and 14 AVFs. A detailed description is given in the Supplement. The 14 AVFs are geographically widespread and diverse (Fig. 1a). If the absolute age distribution of the volcanic rocks is available, the Holocene areas were mapped using the age range from 11.7 ka to the present, according to the International Commission on Stratigraphy version 2017/02 (Cohen et al., 2013). If possible, coordinates of water sample locations were used to constrain the catchment boundary to calculate the Holocene fraction for monitored areas. In all cases, already existing alkalinity flux calculations were taken from Li et al. (2016). Detailed information on additional mapping and calculations for each system can be found in the Supplement (SI).

The weathering reactivity (R) of each volcanic field is calculated by normalizing the observed alkalinity flux of the AVF ($F_{\text{calculated}}$, in $10^6\,\text{mol}\,\text{km}^{-2}\,\text{a}^{-1}$) to that of the expected flux if the AVF would be an IVF (F_{expected}):

$$R = \frac{F_{\text{calculated}}}{F_{\text{expected}}}, \tag{1}$$

where the expected alkalinity flux F_{expected} for IVFs is given by the function (Fig. 1b)

$$F_{\text{expected}}\left[10^6\,\text{mol}\,\text{km}^{-2}\,\text{a}^{-1}\right] = 0.23 \cdot e^{(0.06 \cdot T\,(^\circ\text{C}))}, \quad \text{RMSE} = 0.3. \tag{2}$$

The root mean square error of the function is represented by RMSE. The parameters of the equation were derived by using a Monte Carlo method, simulating 10 000 runs (for more information, see the Supplement).

IVFs group around a reactivity $R = 1$ in Fig. 1c, while having a Holocene fraction of zero. The reactivity R (Eq. 1) of an AVF can be estimated by the Holocene area fraction as implied by the significant linear correlation identified in Fig. 1c. The theoretical reactivity of a 100 % Holocene area H might be estimated by the equation given by Fig. 1c, substituting y and x and setting H to 100:

$$R_{100\%\,\text{Holocene}} = 1 + 0.10 \cdot H = 11. \tag{3}$$

With this, the flux from a young system of only Holocene age is

$$F_{\text{Holocene}} = R_{100\%\,\text{Holocene}} \cdot F_{\text{expected}}. \tag{4}$$

Global alkalinity fluxes from basalt areas were calculated by using Eq. (2) for areas older than Holocene age and Eq. (4) for mapped Holocene areas. These equations (Eq. 2 and the following, using information based on Eq. 2) were calibrated for areas with a runoff $> 74\,\text{mm}\,\text{a}^{-1}$ (the lowest runoff value in the data compilation of Li et al., 2016, and therefore limit of the model setup) to avoid too-high alkalinity fluxes from drier areas with high temperature (e.g., the Sahara), assuming that neglecting fluxes from areas with lower runoff is not biasing the comparison (Table S1). In this case, an overestimation is avoided. For the global calculation of CO_2 consumption by the new scaling law, a Monte Carlo method simulating 10 000 runs was applied (see the Supplement).

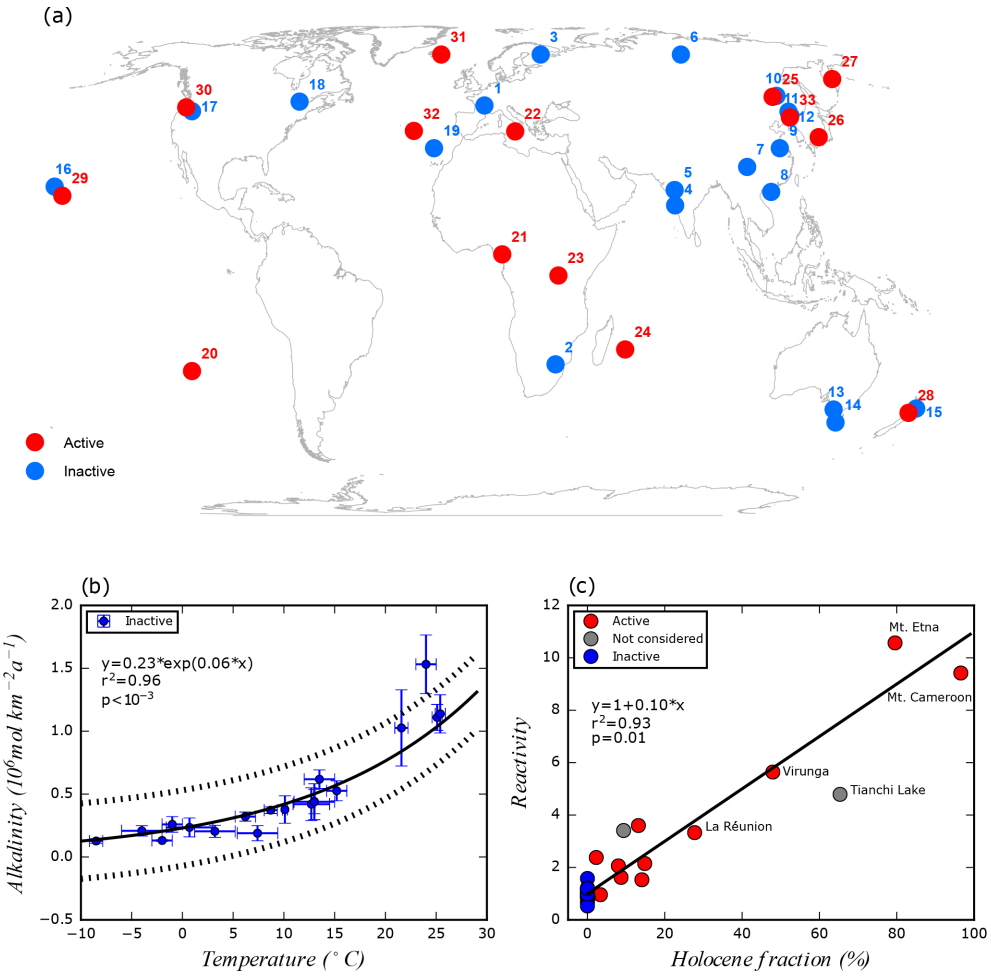

Figure 1. **(a)** The global map shows the locations of the active volcanic fields (in red) and the inactive volcanic fields (in blue) used in this study (1. Massif Central, 2. South Africa, 3. Karelia, 4. coastal Deccan, 5. interior Deccan, 6. Siberian Traps, 7. Mt. Emei, 8. Leiqiong, 9. Nanjing, 10. Xiaoxinganling, 11. Tumen River, 12. Mudan River, 13. southeast Australia, 14. Tasmania, 15. North Island, NZ, 16. Kauai, Hawaii, 17. Columbia Plateau, 18. northeast North America, 19. Madeira Island, 20. Easter Island, 21. Mt. Cameroon, 22. Mt. Etna, 23. Virunga, 24. La Réunion, 25. Wudalianchi Lake, 26. Japan, 27. Kamchatka, 28. Taranaki, 29. Big Island, Hawaii, 30. High Cascades, 31. Iceland, 32. São Miguel Island, 33. Tianchi Lake). **(b)** The exponential relationship between area specific alkalinity flux rates and the land surface temperature for IVFs. The dashed lines represent the range of the mean residual standard deviation of the function (see the Supplement). Note that r^2 and the p value were derived by a linear regression of calculated alkalinity flux rates vs. estimated alkalinity flux rates using the new scaling law. **(c)** The relationship between the Holocene area fraction of the used watersheds from the volcanic fields and the weathering reactivity R. Note that Tianchi Lake and São Miguel are excluded from the calculation of the regression line because the applied catchments were not dominated by basalt but by trachytic volcanic rock types. Both data points still seem to follow the identified regression trend line for AVFs. r^2 and the p value were calculated by a linear regression of the Holocene fraction vs. reactivity for all AVFs.

Results are compared with four previous global empirical alkalinity flux models (Bluth and Kump, 1994; Amiotte-Suchet and Probst, 1995; Dessert et al., 2003; Goll et al., 2014). Alkalinity fluxes were translated into CO_2 consumption to allow for comparison with previous literature. For all models, the same data input was used: a newly compiled global basalt map (mostly derived by the basalt lithological layer from the GLiM but enhanced by mapped Holocene areas (see the Supplement; Hartmann and Moosdorf, 2012), additional regional geological maps describing basalt areas and the maps of the volcanic fields used in this study; for detailed information, see the Supplement), temperature (Hijmans et al., 2005) and runoff (Fekete et al., 2002).

3 Results and discussion

Studied IVFs are characterized by a Holocene volcanic surface area of 0 % with weathering reactivity R ranging between 0.5 and 1.6 (Fig. 1c). In contrast, AVFs show a large range of Holocene coverage, from 0.2 % (High Cascades) to

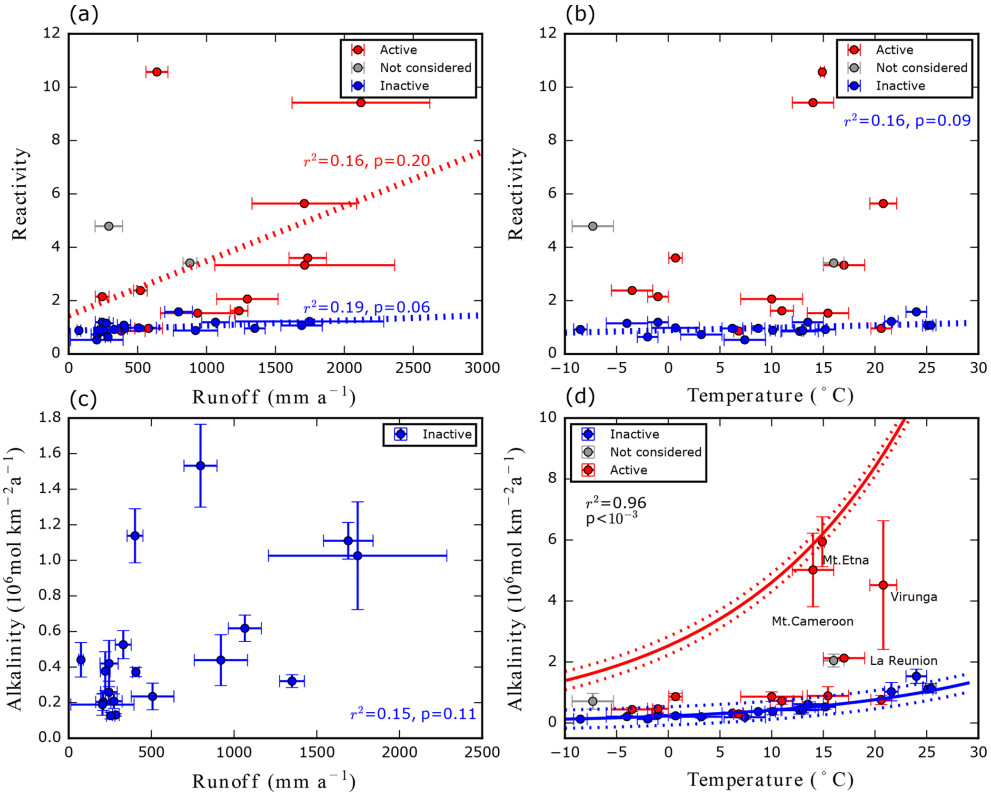

Figure 2. Panel **(a)** shows the runoff–reactivity relationship of all studied volcanic fields. The blue regression line (IVFs) suggests almost no correlation of reactivity with runoff; also, for the AVFs, no significant correlation is identified ($r^2 = 0.16$, $p = 0.20$). **(b)** Reactivity vs. temperature suggests no bias of reactivity due to a temperature effect for AVFs, as reactivity is based on a temperature normalized parameterization. For the IVFs ($r^2 = 0.16$, $p = 0.09$), no bias with temperature can be identified due to the good correlation of alkalinity fluxes with land surface temperature (blue line). **(c)** Runoff vs. alkalinity flux rates for inactive volcanic fields shows no significant correlation ($r^2 = 0.15$, $p = 0.11$). **(d)** Temperature vs. alkalinity flux rates for all volcanic fields of the study. The blue line represents the new scaling law for IVFs and the red line the new scaling law for AVFs with 100 % Holocene area coverage (calculated deviation is represented by dashed lines). r^2 and the p value are derived by a linear regression of calculated alkalinity flux rates vs. observed alkalinity flux rates for all volcanic fields.

96.6 % (Mt. Cameroon), and weathering reactivity between 0.9 (High Cascades) and 10.6 (Mt. Etna). The weathering reactivity correlates strongly with the percentage of Holocene area ($r^2 = 0.93$; Fig. 1c), suggesting Holocene surface area distribution is a good predictor for the enhanced alkalinity fluxes from a volcanic system:

$$F_{\text{alkalinity}} = (1 + 0.10 \cdot H) \cdot 0.23 \cdot e^{(0.06 \cdot T)} \quad [10^6\,\text{mol}\,\text{km}^{-2}\,\text{a}^{-1}], \text{RMSE} = 0.3, \tag{5}$$

where H is the Holocene fraction of a volcanic system in percent and T is land surface temperature in °C.

The Holocene fraction is not interpreted as the physical cause for elevated alkalinity fluxes. Instead, magmatic CO_2 contribution, geothermal–hydrothermal activity and the input of new volcanic material on top of the surface (properties and "freshness" of the surface area for reaction) are contributing to enhanced alkalinity fluxes. Volcanic ashes and ejecta might contribute to elevated weathering fluxes because of a relatively high content of glass. Glass dissolution rates are relatively high compared to mineral dissolution rates in general, but base cation content release varies based on the Si : O ratio (Wolff-Boenisch et al., 2006).

The magmatic CO_2 contributions to alkalinity fluxes in young volcanic systems may be large in general, but data are scarce to evaluate the global relevance for AVFs. For the Lesser Antilles, a magmatic contribution of 23 % to 40 % to the CO_2 consumed by weathering was identified (Rivé et al., 2013). High ^{13}C–dissolved inorganic carbon (DIC) values suggest that magmatic CO_2 contributes significantly to the alkalinity fluxes from the Virunga system (Balagizi et al., 2015). The magmatic CO_2 contribution derived from volcanic calcite dissolution in Iceland was estimated to be about 10 % of the alkalinity fluxes for the studied area (Jacobson et al., 2015). In the case of Mt. Etna, 7 % of the CO_2 emitted due to volcanic activity may be captured by weathering (Aiuppa et al., 2000). These examples suggest that signifi-

Table 1. Summary of global basalt CO_2 consumption rates for different models and the new parameterization. For simplicity, it was assumed that alkalinity fluxes equal CO_2 consumption. The percentiles of the values of the global calculation by the new scaling law (Monte Carlo method) can be found in the Supplement. The standard deviation is given below as described in the Supplement.

Models for comparison	Parameters	Global CO_2 consumption rate (10^9 mol a^{-1}) for limited area in comparison (only areas with $>$ 74 mm a^{-1} runoff)	Global CO_2 consumption rate (10^9 mol a^{-1})
Dessert et al. (2003)	Runoff, temperature	1669	1684
Amiotte-Suchet and Probst (1995)	Runoff	863	870
Bluth and Kump (1994)	Runoff	746	761
Goll et al. (2014)	Runoff, temperature	1566	1580
New scaling law	Temperature	1930 ± 90	3300 ± 200

cant amounts of magmatic carbon may be transferred to the ocean directly via intravolcanic weathering from AVFs.

These examples show that in the case of active volcanic fields the traditional view on kinetic vs. supply limitation in the "shallow" critical zone in context of tectonic settings does not hold (e.g., Ferrier et al., 2016). In contrast, the supply of fresh material on top of the classical critical zone and the weathering from below the classical critical zone suggest that these hot spots of silicate weathering in active volcanic areas, which contribute over proportionally to the global CO_2 consumption by silicate weathering, demand likely a different way of looking at it. The blue data points (IVFs) in Fig. 2d suggest a kinetic-limited regime and follow a temperature dependency. The red points (AVFs) however are located above the data points of IVFs in general. Taking into account that the four AVFs (Mt. Etna, Mt. Cameroon, Virunga and La Réunion) have the highest Holocene fractions (96.6 %–27.7 %) and that the further AVFs, which have less than 15 % Holocene coverage, are located in general above the regression line for IVFs, supports the argument that a combination of elevated geothermal fluxes, magmatic CO_2 and fresh material supplied on top of the classical critical zone contributes to the observed elevated alkalinity fluxes for AVFs in general.

The calculated global basalt weathering alkalinity fluxes based on previous global models (Bluth and Kump, 1994; Amiotte-Suchet and Probst, 1995; Dessert et al., 2003; Goll et al., 2014) give alkalinity fluxes ranging between 0.8 and 1.7×10^{12} mol a^{-1}. These values are different from previously published results based on the same models because a different geological map and climate data are used in this study. The new scaling law calculation based on the temperature dependence of weathering rate and the age dependence of weathering reactivity (Eq. 4) results in higher global alkalinity fluxes of 1.9×10^{12} and 3.3×10^{12} mol a^{-1} for regions with > 74 mm a^{-1} runoff and for all areas, respectively. The latter higher estimate is mainly due to the modeled contribution from dry and hot regions and shows that it is relevant to apply the runoff cutoff.

Using the introduced new approach, considering the aging of a volcanic system, reveals that alkalinity fluxes from Holocene areas contribute today only 5 % to the global basalt weathering alkalinity flux. This is because so far identified mapped Holocene volcanic areas cover only ~ 1 % of all basalt areas. This study did not include areas of less mafic volcanic areas, like andesites, or Central American volcanics.

The Holocene area is probably underestimated due to information gaps in the reported age information of the global map. The strong dependence of weathering reactivity on relative age of the surface of a considered volcanic system suggests that it is relevant to know the global spatial age distribution of volcanic areas in more detail. Therefore, a new global review of the age distribution of basalt areas would be needed, which is beyond the scope of this study. The lithologies, predominantly described as basaltic in the global map, might introduce an additional bias to the global calculations because heterogeneities in the lithology cannot be excluded. Two active volcanic fields (São Miguel and Tianchi Lake) were excluded from the calculation of the scaling law function because available catchments with alkalinity data hold large areas with lithologies of trachytic composition. Nevertheless, their data points (Fig. 1c) seem to show the same weathering behavior.

The applied time period of the Holocene boundary suggests that the aging of the "weathering motor" of a basaltic volcanic area, including internal weathering, with declining volcanic activity is rather rapid. This implies that peaks in global volcanic activity have probably a short but intensive effect on the CO_2 consumption. A pronounced effect on the global carbon cycle by shifting the global reactivity of volcanic areas may only be relevant for geological periods with significantly elevated production of new volcanic areas, accompanied by geothermal–hydrothermal activity and capture of magmatic CO_2 before its escape to the atmosphere.

Results may have relevance for the carbon cycle and climate studies exploring the emplacement of large igneous provinces like the CAMP (Schaller et al., 2012) or the Deccan Traps (Caldeira and Rampino, 1990) with production of large basaltic areas within a short time. However, the biological contribution to CO_2 drawdown, via elevated fertilization

effects, e.g., P or Si release due to weathering and elevated CO_2 in the atmosphere, should be taken into account, too.

Looking deeper into Earth's history: variations in the solid Earth CO_2 degassing rate or changes in environmental conditions affecting the weathering intensity (Teitler et al., 2014; Hartmann et al., 2017) may have caused different reactivity patterns in dependence of surface age as shown here.

In conclusion, a simple approach to detect an aging effect, using surface age as a proxy for several combined processes, was chosen due to availability of data. It can be shown that there exists a linear relationship between temperature-normalized alkalinity fluxes and the Holocene area fraction of a volcanic system. Nevertheless, the combined effect on elevated weathering reactivity due to magmatic CO_2 contribution, hydrothermal activity, production of fresh surface area for reaction and hydrological factors of young volcanic systems remains to be disentangled, for single volcanic systems, as well as for the emplacement of larger, trap-style basalt areas.

Supplement. The supplement related to this article is available online at: https://doi.org/10.5194/esurf-7-191-2019-supplement.

Competing interests. The authors declare that they have no conflict of interest.

Author contributions. The study was designed by the authors, the mapping was done by JB and the calculations were done by JB and GRM. The text was written by all authors.

Acknowledgements. Funding for this work has been provided by German Research Foundation (DFG) through the Cluster of Excellence CLISAP2 (DFG Exec177, Universität Hamburg) and BMBF-project PALMOD (ref. 01LP1506C) through the German Federal Ministry of Education and Research (BMBF) as part of the Research for Sustainability initiative (FONA). Gaojun Li is supported by National Natural Science Foundation of China (grants 41761144058 and 41730101). The authors thank the editor, Robert Emberson, and one anonymous reviewer for constructive comments on the manuscript.

Edited by: Heather Viles
Reviewed by: Robert Emberson and one anonymous referee

References

Aiuppa, A., Allard, P., D'Alessandro, W., Michel, A., Parello, F., Treuil, M., and Valenza, M.: Mobility and fluxes of major, minor and trace metals during basalt weathering and groundwater transport at Mt. Etna volcano (Sicily), Geochim. Cosmochim. Acta, 64, 1827–1841, 2000.

Amiotte-Suchet, P. and Probst, J. L.: A global model for present-day atmospheric/soil CO_2 consumption by chemical erosion of continental rocks (GEM-CO_2), Tellus B, 47, 273–280, https://doi.org/10.1034/j.1600-0889.47.issue1.23.x, 1995.

Balagizi, C. M., Darchambeau, F., Bouillon, S., Yalire, M. M., Lambert, T., and Borges, A. V.: River geochemistry, chemical weathering, and atmospheric CO_2 consumption rates in the Virunga Volcanic Province (East Africa), Geochem. Geophys. Geosyst., 16, 2637–2660, https://doi.org/10.1002/2015GC005999, 2015.

Berner, R. A., Lasaga, A. C., and Garrels, R. M.: The carbonate-silicate geochemical cycle and its effect on atmospheric carbon dioxide over the past 100 million years, Am. J. Sci., 283, 641–683, 1983.

Bluth, G. J. and Kump, L. R.: Lithologic and climatologic controls of river chemistry, Geochim. Cosmochim. Acta, 58, 2341–2359, 1994.

Caldeira, K. and Rampino, M. R.: Carbon dioxide emissions from Deccan volcanism and a K/T boundary greenhouse effect, Geophys. Res. Lett., 17, 1299–1302, 1990.

Cohen, K., Finney, S., Gibbard, P., and Fan, J.-X.: The ICS international chronostratigraphic chart, Episodes, 36, 199–204, 2013.

Coogan, L. A. and Dosso, S. E.: Alteration of ocean crust provides a strong temperature dependent feedback on the geological carbon cycle and is a primary driver of the Sr-isotopic composition of seawater, Earth Planet. Sci. Lett., 415, 38–46, https://doi.org/10.1016/j.epsl.2015.01.027, 2015.

Dessert, C., Dupré, B., François, L. M., Schott, J., Gaillardet, J., Chakrapani, G., and Bajpai, S.: Erosion of Deccan Traps determined by river geochemistry: impact on the global climate and the 87Sr/86Sr ratio of seawater, Earth Planet. Sci. Lett., 188, 459–474, https://doi.org/10.1016/S0012-821X(01)00317-X, 2001.

Dessert, C., Dupré, B., Gaillardet, J., François, L. M., and Allègre, C. J.: Basalt weathering laws and the impact of basalt weathering on the global carbon cycle, Chem. Geol., 202, 257–273, https://doi.org/10.1016/j.chemgeo.2002.10.001, 2003.

Fekete, B. M., Vörösmarty, C. J., and Grabs, W.: High-resolution fields of global runoff combining observed river discharge and simulated water balances, Global Biogeochem. Cy., 16, 15-1–15-10, https://doi.org/10.1029/1999gb001254, 2002.

Ferrier, K. L., Riebe, C. S., and Jesse Hahm, W.: Testing for supply-limited and kinetic-limited chemical erosion in field measurements of regolith production and chemical depletion, Geochem. Geophys. Geosyst. 17, 2270–2285, 2016.

Gaillardet, J., Dupré, B., Louvat, P., and Allègre, C. J.: Global silicate weathering and CO_2 consumption rates deduced from the chemistry of large rivers, Chem. Geol., 159, 3–30, https://doi.org/10.1016/S0009-2541(99)00031-5, 1999.

Gaillardet, J., Rad, S., Rivé, K., Louvat, P., Gorge, C., Allègre, C. J., and Lajeunesse, E.: Orography-driven chemical denudation in the Lesser Antilles: Evidence for a new feed-back mechanism stabilizing atmospheric CO_2, Am. J. Sci., 311, 851–894, 2011.

Goddéris, Y., Donnadieu, Y., Nédélec, A., Dupré, B., Dessert, C., Grard, A., Ramstein, G., and François, L. M.: The Sturtian "snowball" glaciation: fire and ice, Earth Planet. Sci. Lett., 211, 1–12, https://doi.org/10.1016/S0012-821X(03)00197-3, 2003.

Goll, D. S., Moosdorf, N., Hartmann, J., and Brovkin, V.: Climate-driven changes in chemical weathering and associated phosphorus release since 1850: Implications for the

land carbon balance, Geophys. Res. Lett., 41, 3553–3558, https://doi.org/10.1002/2014GL059471, 2014.

Hartmann, J. and Moosdorf, N.: The new global lithological map database GLiM: A representation of rock properties at the Earth surface, Geochem. Geophys. Geosyst., 13, Q12004, https://doi.org/10.1029/2012gc004370, 2012.

Hartmann, J., Jansen, N., Dürr, H. H., Kempe, S., and Köhler, P.: Global CO_2-consumption by chemical weathering: What is the contribution of highly active weathering regions?, Global Planet. Change, 69, 185–194, 2009.

Hartmann, J., Li, G., and West, A. J.: Running out of gas: Zircon 18O-Hf-U/Pb evidence for Snowball Earth preconditioned by low degassing, Geochem/ Perspect/ Lett/, 4, 41–46, https://doi.org/10.7185/geochemlet.1734, 2017.

Hijmans, R. J., Cameron, S. E., Parra, J. L., Jones, P. G., and Jarvis, A.: Very high resolution interpolated climate surfaces for global land areas, Int. J. Climatol., 25, 1965–1978, 2005.

Jacobson, A. D., Grace Andrews, M., Lehn, G. O., and Holmden, C.: Silicate versus carbonate weathering in Iceland: New insights from Ca isotopes, Earth Planet. Sci. Lett., 416, 132–142, https://doi.org/10.1016/j.epsl.2015.01.030, 2015.

Kent, D. V. and Muttoni, G.: Modulation of Late Cretaceous and Cenozoic climate by variable drawdown of atmospheric pCO_2 from weathering of basaltic provinces on continents drifting through the equatorial humid belt, Clim. Past, 9, 525–546, https://doi.org/10.5194/cp-9-525-2013, 2013.

Li, G. and Elderfield, H.: Evolution of carbon cycle over the past 100 million years, Geochim. Cosmochim. Acta, 103, 11–25, https://doi.org/10.1016/j.gca.2012.10.014, 2013.

Li, G., Hartmann, J., Derry, L. A., West, A. J., You, C.-F., Long, X., Zhan, T., Li, L., Li, G., Qiu, W., Li, T., Liu, L., Chen, Y., Ji, J., Zhao, L., and Chen, J.: Temperature dependence of basalt weathering, Earth Planet. Sci. Lett., 443, 59–69, https://doi.org/10.1016/j.epsl.2016.03.015, 2016.

Rad, S., Rivé, K., Vittecoq, B., Cerdan, O., and Allègre, C. J.: Chemical weathering and erosion rates in the Lesser Antilles: An overview in Guadeloupe, Martinique and Dominica, J. South Am. Earth Sci., 45, 331–344, https://doi.org/10.1016/j.jsames.2013.03.004, 2013.

Rivé, K., Gaillardet, J., Agrinier, P., and Rad, S.: Carbon isotopes in the rivers from the Lesser Antilles: origin of the carbonic acid consumed by weathering reactions in the Lesser Antilles, Earth Surf. Process. Landf., 38, 1020–1035, https://doi.org/10.1002/esp.3385, 2013.

Schaller, M. F., Wright, J. D., Kent, D. V., and Olsen, P. E.: Rapid emplacement of the Central Atlantic Magmatic Province as a net sink for CO_2, Earth Planet. Sci. Lett., 323–324, 27–39, https://doi.org/10.1016/j.epsl.2011.12.028, 2012.

Taylor, A. and Blum, J. D.: Relation between soil age and silicate weathering rates determined from the chemical evolution of a glacial chronosequence, Geology, 23, 979–982, 1995.

Teitler, Y., Le Hir, G., Fluteau, F., Philippot, P., and Donnadieu, Y.: Investigating the Paleoproterozoic glaciations with 3-D climate modeling, Earth Planet. Sci. Lett., 395, 71–80, https://doi.org/10.1016/j.epsl.2014.03.044, 2014.

Walker, J. C. G., Hays, P. B., and Kasting, J. F.: A negative feedback mechanism for the long-term stabilization of Earth's surface temperature, J. Geophys. Res.-Oceans, 86, 9776–9782, https://doi.org/10.1029/JC086iC10p09776, 1981.

Wolff-Boenisch, D., Gislason, S. R., and Oelkers, E. H.: The effect of crystallinity on dissolution rates and CO_2 consumption capacity of silicates, Geochim. Cosmochim. Acta, 70, 858–870, 2006.